Chapter 2

# THE DISTRIBUTED HYDROLOGY SOIL VEGETATION MODEL

**Mark S. Wigmosta[1], Bart Nijssen[2], and Pascal Storck[1]**

[1] Pacific Northwest National Laboratory, Richland, Washington
[2] University of Washington, Seattle, Washington

## ABSTRACT

The use of distributed physically based models in environmental analysis is becoming more common as greater demands are placed on hydrologic models, particularly for problems involving prediction of future hydrologic conditions resulting from changes in land use or climate. The Distributed Hydrology Soil Vegetation Model (DHSVM) is a physically based model that provides a dynamic representation of the spatial distribution of evapotranspiration, snow cover, soil moisture, and runoff at the spatial scale of digital elevation model data. The model has evolved significantly over the last several years to enable it to address a wide range of applied and research activities. This chapter presents a description of the current state of the model including field test results and example applications.

## 2.1. INTRODUCTION

As the demands placed on hydrologic models for environmental decision making has increased, the use of distributed physically based models is becoming more common. Where it once may have been sufficient to estimate catchment outflow, many applications now require an accurate representation of the spatial and temporal patterns of runoff production and the associated transport pathways of water, sediment,

chemicals, and nutrients. Although most hydrologic analysis is still performed using lumped conceptual models, physically based process models are better suited for many problems, particularly those involving the prediction of future hydrologic conditions produced by changes in land use or climate when no data are available for calibration. Distributed models are also better suited to utilize current spatial data products (e.g., NEXRAD rainfall and AVHRR snow cover data), or real-time point measurements (such as Snotel air temperature, soil moisture, and snow water equivalent) for input and testing. This disparity between distributed process based and lumped conceptual models will only worsen in the future as more advanced sensor technologies come online.

The Distributed Hydrology Soil Vegetation Model (DHSVM) is a physically based distributed parameter model that provides an integrated representation of watershed processes at the spatial scale described by digital elevation model (DEM) data. DHSVM has been utilized in a number of research activities involving hydrologic analysis and modeling (Wigmosta et al., 1994; Haddeland and Lettenmaier, 1995; Kenward and Lettenmaier, 1997; Wigmosta and Lettenmaier, 1999; Westrick et al., 2000). The model has also been used to study the interactions between climate and hydrology (Wigmosta et al., 1995; Arola and Lettenmaier, 1996; Nijssen et al., 1997) and the potential impacts of climate change on water resources (Leung et al., 1996; Leung and Wigmosta, 1999; Wigmosta and Leung, 2000). There has been significant use of the model for basic and applied research concerning forest management activities on watershed processes (Storck et al., 1995, Lamarche and Lettenmaier, 1998; Storck et al., 1998; Storck et al., 1999; Bowling et al., 2000; Storck, 2000; Bowling and Lettenmaier, 2001; Wigmosta and Perkins, 2001).

The model has evolved significantly from the original version described in Wigmosta et al. (1994). Canopy snow interception and release is now simulated. A more accurate two-layer ground snowpack representation has replaced the original one-layer representation. A three-dimensional overland flow representation has been added, as well as the ability to simulate the impacts of roads on downslope water redistribution. A one-dimensional channel flow model has been added along with other improvements. This chapter presents a relatively detailed description of the current state of the model along with field test results and example applications.

## 2.2. MODEL DESCRIPTION

DHSVM provides a dynamic representation of watershed processes at the spatial scale described by Digital Elevation Model (DEM) data (typically 10 - 90 m horizontal resolution). The modeled landscape is divided into computational grid cells centered on DEM nodes Fig. 2.1. This characterization of topography is used to model topographic controls on absorbed shortwave radiation, precipitation, air temperature, and downslope water movement. Vegetation characteristics and soil properties are assigned to each model grid cell. These properties may vary spatially throughout the basin. In each grid cell the modeled land surface can be composed of a combination of vegetation and soil. At each time step, the model provides simultaneous solutions to energy and water balance equations for every grid cell in the watershed. Individual grid cells are hydrologically linked through surface and subsurface flow routing.

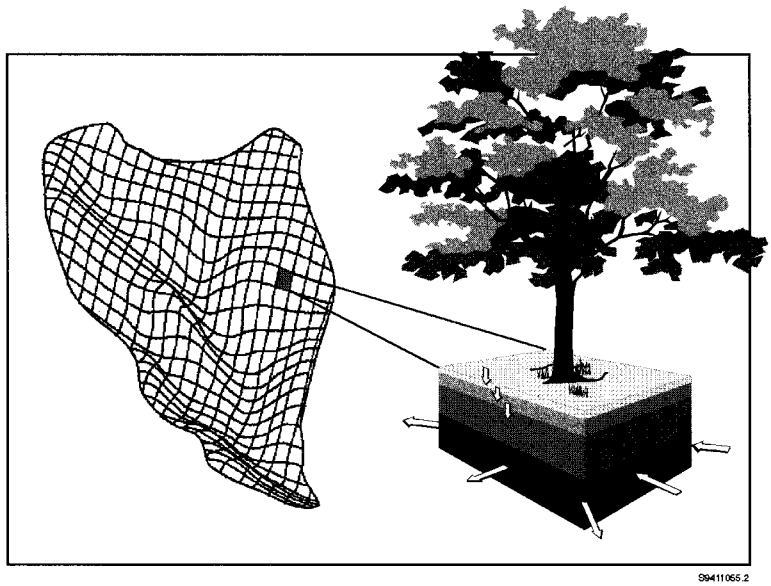


**Fig. 2.1. Model representation of a watershed. DEM data are used to model topographic controls on absorbed solar radiation, precipitation, air temperature, and downslope water movement. Grid cells are allowed to exchange water with their adjacent neighbors, resulting in a three-dimensional redistribution of surface and subsurface water across the landscape (adapted from Wigmosta et al., 1994).**

Canopy snow interception and release is modeled using a one-layer mass- and energy balance model. Snow accumulation and melt below the canopy (or in the open) are simulated using a two-layer mass- and energy-balance model that explicitly incorporates the effects of topography and vegetation cover on the energy and mass exchange at the snow surface. Evapotranspiration is represented using a two-layer canopy model with each layer partitioned into wet and dry areas. Unsaturated moisture movement through multiple rooting zone soil layers is calculated using Darcy's Law. Discharge from the lower rooting zone recharges the local (grid cell) water table (Fig. 2.2). Each

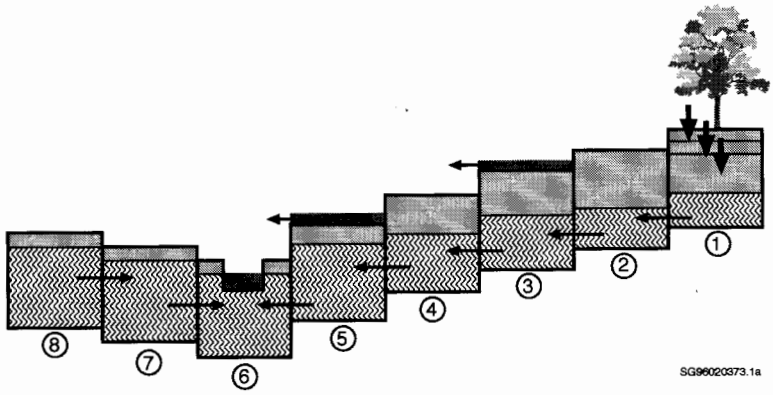


**Fig. 2.2. Model representation of downslope water movement to a stream channel. Dark shading represents surface water in the form of overland flow (model cells 3 and 5) or as channel flow (model cell 6). Light shading represents unsaturated soil, while the wave pattern corresponds to saturated soil below the water table. In each grid cell, percolation from the lower rooting zone recharges local grid cell water tables (shown by the downward arrows in cell 1). Grid cells exchange water with adjacent neighbors resulting in the downslope movement of water (horizontal arrows) to stream channels. The stream channel receives subsurface flow when grid cell water tables rise above the elevation of the channel bed (model cell 6). Surface flow may be reinfiltrated in downslope grid cells where the zone of soil saturation is below the ground surface (surface flow from cells 3 and 5 reinfiltrate in cells 4 and 6, respectively).**

grid cell exchanges water with its adjacent neighbors as a function of local hydraulic conditions resulting in a transient, three-dimensional representation of surface and saturated subsurface flow. Return flow and saturation overland flow are generated in locations where grid cell water tables intersect the ground surface.

The drainage network is represented as a series of connected reaches with each reach passing through one or more DEM grid cells. As surface and subsurface water is routed downslope toward a stream channel it may be intercepted by a road network. A road reach begins to intercept subsurface flow when grid cell water tables rise above the elevation of the associated road drainage ditches. Surface water in roadside ditches is routed through the road drainage network until it reaches a culvert or stream channel. If the road intersects a stream channel, the water is input to the appropriate channel reach and routed through the channel system. The discharge from a culvert without a defined channel is allowed to reinfiltrate as it moves downslope below the culvert. The active road drainage/channel network may expand and contract as grid cell water tables rise and fall below their channel beds. Flow in road drainage ditches and stream channels is routed using a cascade of linear channel reservoirs.

The Geographical Information System (GIS) ARC/INFO is used to automate model setup and facilitate the analysis of model output. ARC/INFO is used to delineate watershed boundaries and build a DEM consistent with other hydrologic information, such as the stream network. The GIS is used to assign spatially distributed model input parameters to DEM grid cells using overlays of soils, vegetation, roads (including culvert locations), and stream channels. ARC/INFO macros are used to subdivide the road and stream network into reaches and calculate local slopes and flow directions for each segment. ARC/INFO is also used to order reaches in the channel and road drainage networks for proper flow routing. The seven modules that represent the DHSVM coupled water and energy balance, specifically evapotranspiration, snowpack accumulation and melt, canopy snow interception and release, unsaturated moisture movement, saturated subsurface flow, surface overland flow, and channel flow are described in sections 2.3-2.9.

## 2.3. EVAPOTRANSPIRATION

An individual grid cell may contain an overstory canopy and either an understory or bare soil. Both the understory and the overstory may contain wet and dry fractions. The overstory, if present, may cover all or a prescribed fraction of the cell area, while the understory or bare soil covers the entire cell. When a ground snowpack is present, it is assumed to completely cover the understory or soil. As a result the understory or soil does not contribute evapotranspiration when a ground snowpack is present.

Potential evaporation is first calculated for the overstory and represents the maximum rate that water can be removed from the cell vegetation and soil via evapotranspiration. Water intercepted by the overstory is then removed from the wet fraction at the potential rate, while transpiration from the dry fraction is modeled using a Penman-Monteith approach. The calculated overstory evapotranspiration (both wet and dry fractions) is then subtracted from the potential evaporation and understory evapotranspiration is calculated from the modified potential evaporation rate. This stepwise approach allows the wet fractions of both canopies to dry during a time step (i.e., evaporation followed by transpiration), while insuring the total evapotranspiration from both layers does not exceed the amount of moisture the atmosphere can absorb (i.e., the rate of potential evaporation for the overstory).

The rate of potential evaporation for the overstory ( $E_{po}$) is given by (Wigmosta et al., 1994)

$$E_{po} = \frac{\Delta R_{no} + \rho c_p (e_s - e) / r_{ao}}{\lambda_v [\Delta + \gamma]} \tag{2.1}$$

where $\Delta$ is the slope of the saturated vapor pressure - temperature curve, $R_{no}$ is the net radiation flux density, $\rho$ is the density of moist air, $c_p$ is the specific heat of air at constant pressure, $e_s$ is the saturation vapor pressure at the air temperature, $e$ is the vapor pressure, $r_{ao}$ is the aerodynamic resistance to vapor transport between the overstory and the reference height, $\lambda_v$ is the latent heat of vaporization of water, and $\gamma$ is the psychrometric constant. Transpiration from dry vegetative surfaces is calculated using a Penman-Monteith approach (Wigmosta et al., 1994)

$$E_{tj} = E_{pj} \frac{\Delta + \gamma}{\Delta + \gamma\left(1 + r_{cj}/r_{aj}\right)} \tag{2.2}$$

where $E_{tj}$ is the transpiration rate, $E_{pj}$ is the appropriate rate of potential evaporation, and $r_{cj}$ is the canopy resistance to vapor transport. Each canopy layer is partitioned into a wet fraction ($A_{wj}$) and a dry fraction (1-$A_{wj}$) following Deardorff (1978) and Dickinson et al. (1993), with

$$A_{wj} = \left( \frac{S_{Ij}^{t} + P_j}{I_{cj}} \right)^{2/3} \tag{2.3}$$

where $S_{Ij}^{t}$ is the depth of intercepted water stored on the canopy at the start of the time step, $P_j$ is the depth of rainfall during the time step. $I_{cj}$ is the maximum interception storage capacity (in meters), determined from projected Leaf Area Index (LAI); with $I_{cj} = r_j LAI_j F_j$, where $r_j$ is the ratio of $I_{cj}$ to $LAI_j$ (typically about $10^{-4}$, Dickinson et al., 1991), and $F_j$ is the fraction of ground surface covered by the canopy. Rainfall is stored on the surface of each canopy until its maximum interception storage capacity is reached. Any excess precipitation passes through the canopy as throughfall with no attenuation. $P$ is equal to the overstory throughfall when Eq. (2.3) is applied to the understory ($j = 2$).

The model calculates evaporation and transpiration independently for each layer in a stepwise fashion. First, water from the wet fraction is evaporated at the potential rate

$$E_{Ij} = E_{pj} A_{wj} \Delta t_w \tag{2.4}$$

where $E_{Ij}$ is the amount of intercepted water evaporated over the time period and $\Delta t_w$ is the time required to evaporate the intercepted water at the potential rate. If the potential rate is insufficient to remove all of the intercepted water during the model time step, $\Delta t_w$ equals the length of the model time step ($\Delta t$). The total transpiration from dry vegetation ($E_{Tj}$) is then calculated using Eq. (2.2), Eq. (2.3), and $\Delta t_w$

$$E_{Tj} = E_{tj}\left(1 - A_{wj}\right)\Delta t + E_{tj} A_{wj}\left(\Delta t - \Delta t_w\right) \tag{2.5}$$

In the application of Eq. (2.2) - (2.5), $E_{pj} = E_{po}$ for the overstory and $E_{pj} = E_{po} - (E_{Io} + E_{To})$ for the understory, with $E_{po}$ calculated through Eq. (2.1).

Evaporation from the upper soil layer is simulated in the absence of an understory, otherwise soil evaporation is ignored. When wet, a soil may be able to supply water to the surface at a rate equal to or greater than the potential evaporation demand. As soil moisture is depleted, the rate of delivery falls below the potential evaporation rate. At this and lower moisture states, the evaporation rate is soil-controlled and is a nonlinear function of the soil moisture content. Under this approach, soil water evaporation $(E_s)$ is calculated as

$$E_s = \min(E_{ps}, Fe) \tag{2.6}$$

where $E_{ps} = E_{po} - (E_{Io} + E_{To})$ and $F_e$ is the soil desorptivity, determined by the rate at which the soil can deliver water to the surface. Desorptivity is a function of soil type and moisture conditions in the upper soil zone and is discussed in section 2.4.2.

### 2.3.1. Aerodynamic Resistance

The vertical wind profile through the overstory canopy is modeled assuming neutral atmospheric conditions using three layers (Storck, 2000). The wind profile above the canopy is represented using a logarithmic profile from the reference height down to the top of a roughness sublayer just above the overstory canopy. This sublayer extends down to the overstory canopy displacement height. The wind profile through the remainder of the overstory is assumed to be exponential. Within the trunk space below the overstory canopy the wind profile is again assumed to be logarithmic.

The total aerodynamic resistance to turbulent transport associated with the three overstory wind profile layers is given by (Storck, 2000):

$$R_{ao} = \frac{\ln\left(\frac{z_r - d_o}{z_{0o}}\right)}{U_r k^2} \left\{ \frac{h_o}{n(z_w - d_o)} \left[ \exp\left( n_a \left( 1 - \frac{d_o - z_{0o}}{h_o} \right) \right) - 1 \right] + \frac{z_w - h_o}{z_w - d_o} + \ln\left(\frac{z_r - d_o}{z_w - d_o}\right) \right\} \tag{2.7}$$

where $U_r$ is the velocity at the reference height $z_r$; $h_o$, $d_o$, $z_{0,o}$ are the height, displacement height, and roughness of the overstory; $z_w$ is the height of the boundary between the upper logarithmic profile and roughness sublayer; $n_a$ is a dimensionless extinction coefficient; and $k$ is Von Karmen's constant. The aerodynamic resistance for the soil surface, snow, or understory associated with the lower logarithmic profile is given by (Storck, 2000):

$$r_{au} = \ln\left(\frac{z_a - d_u}{z_{0u}}\right)^2 \Big/ U(z_a)\, k^2 \tag{2.8}$$

where $z_a = 2 + d_u + z_{0u}$ with $d_u$ and $z_{0u}$ equal to the displacement and roughness height, respectively, for the understory, soil surface, or snow surface.

## 2.3.2. Canopy Resistance

Canopy resistance ($r_{cj}$) is calculated separately for the overstory and understory following the general approach of Wigmosta et al. (1994). For both stories $r_{cj}$ is represented as a summation of the stomatal resistance, $r_{sj}$ of individual leaves. The leaves are assumed to contribute in parallel so that

$$r_{cj} = \langle r_{sj} \rangle / c_j LAI_j \tag{2.9}$$

where $c_j$ is the appropriate ratio of total to projected (one-sided) LAI and the angled brackets denote an inverse average over the range of the canopy leaf area index (Dickinson et al., 1991). The dependence of $r_{sj}$ on vegetation type and environmental factors is represented by a species-dependent minimum resistance ($r_{s\min_j}$) and a product of four limiting factors each with a minimum value of one

$$r_{sj} = r_{s\min_j} f_1(T_j) f_2(vpd_j) f_3(PAR_j) f_4(\theta_j) \tag{2.10}$$

where the environmental dependencies are $f_1$, air temperature; $f_2$, vapor pressure deficit; $f_3$, photosynthetically active radiation flux; and $f_4$,

soil moisture. Relations for the first three of these factors are taken from Dickinson et al. (1993) as

$$f_1 = \left[0.08T_a - 0.0016T_a^2\right]^{-1} \tag{2.11}$$

$$f_2 = \left[1 - \left(e_s - e\right)/e_c\right]^{-1} \tag{2.12}$$

$$f_3 = \frac{1 + R_p/R_{pc}}{r_{s\min}/r_{s\max} + R_p/R_{pc}} \tag{2.13}$$

where $T_a$ is the air temperature (in degrees Celsius), $e_c$ is the vapor pressure deficit causing stomatal closure (about 4 kPa), $r_{s\max}$ is the maximum (cuticular) resistance, $R_p$ is the visible radiation, and $R_{pc}$ is the light level where $r_s$ is twice the minimum stomatal resistance ($r_{s\min}$). Following Feddes et al. (1978), $f_4$ is modeled as a piecewise linear function of soil moisture

$$\begin{aligned} f_4 &= 0 && \theta \le \theta_{wp} \\ f_4 &= \frac{\theta^* - \theta_{wp}}{\theta - \theta_{wp}} && \theta_{wp} < \theta \le \theta^* \\ f_4 &= 1 && \theta^* < \theta \le \theta_s \end{aligned} \tag{2.14}$$

where $\theta$ is the average soil moisture content, $\theta_{wp}$ is the plant wilting point, and $\theta^*$ is the moisture content above which soil conditions do not restrict transpiration.

### 2.3.3. Shortwave and Longwave Radiation

Separate shortwave and longwave radiation budgets are developed for the overstory and the understory or soil surface. The overstory receives direct solar (shortwave) radiation, and exchanges longwave radiation with both the sky and with the understory, snowpack, or soil. The net radiation absorbed by the overstory ($R_{no}$) is given by

$$R_{no} = R_s\left[\left(1-\alpha_o\right)-\tau_o\left(1-\alpha_u\right)\right]F+\left(L_d+L_u-2L_o\right)F \qquad (2.15)$$

where $R_s$ is the incident shortwave radiation supplied to the model, $\alpha_o$ is the overstory reflection coefficient, $\tau_o$ is the fraction of shortwave radiation transmitted by the overstory canopy, $\alpha_u$ is the understory reflection coefficient, $F$ is the fractional ground cover of the overstory, and $L_d$, $L_u$, and $L_o$ are downward sky, upward understory, and overstory longwave radiation fluxes. The fraction of transmitted shortwave radiation is calculated following a Beer's Law relationship of the form (Monteith and Unsworth, 1990)

$$\tau_o = \exp\left(-k_b LAI_o\right) \qquad (2.16)$$

where $k_b$ is a canopy attenuation coefficient, and $\mathrm{LAI}_o$ is the one-sided leaf area index of the overstory canopy.

The understory receives attenuated shortwave radiation below the overstory and direct shortwave radiation in the open. Below the overstory, the understory exchanges longwave radiation with the overstory, while in the open it exchanges radiation with the sky and ground. The net radiation absorbed by the understory $(R_{nu})$ is

$$R_{nu} = R_s\left(1-\alpha_u\right)\left(\left[1-F\right]+\tau_o F\right)+(1-F)L_d+FL_o-L_u \qquad (2.17)$$

Assuming an emissivity of unity, $L_o = \sigma\left(T_o+273\right)^4$ and $L_u = \sigma\left(T_u+273\right)^4$ where $\sigma$ is the Stefan-Boltzmann constant, and $T_o$ and $T_u$ are the temperatures (C) of the overstory and understory, respectively. These two temperatures are set equal to the air temperature except when snow is present, in which case they are determined by energy balance solutions described in sections 2.4 and 2.5. Longwave radiation from the sky is supplied to the model. With bare soil (no understory) and no snowpack, $L_u = \sigma\left(T_g+273\right)^4$ with $T_g$ equal to the soil surface temperature. The soil surface temperature is either set equal to the air temperature or when more accurate surface temperatures are required, calculated through an iterative solution to the nonlinear equation for surface temperature.

## 2.4. TWO-LAYER GROUND SNOWPACK MODEL

Accumulation and melt of the ground snowpack are simulated using the two-layer, energy- and mass-balance model described by Storck and Lettenmaier (1999) and Storck (2000). The energy-balance components are used to simulate snowmelt, refreezing, and changes in the snowpack heat content. The mass-balance components represent snow accumulation/ablation, changes in snow water equivalent, and water yield from the snowpack. The snowpack receives water in both liquid ($P_L$) and solid ($P_I$) phases. In cells without an overstory canopy this is simply the depths of rainfall ($P_r$) and snowfall ($P_s$), respectively; i.e., $P_L = P_r$ and $P_I = P_s$. The delivery process is more complex with the presence of an overstory canopy where some rainfall and snowfall are intercepted by the canopy, some mass may be lost through sublimation, and water may be delivered to the ground snowpack through canopy meltwater drip, mass release, and throughfall. These canopy processes are discussed in section 2.3, with $P_L$ and $P_I$ given by Eq. (2.23) and Eq. (2.24), respectively.

### 2.4.1. Snow Accumulation and Melt

The snowpack is modeled as two layers: a thin surface layer and a lower pack layer. Energy exchange between the atmosphere, overstory canopy, and snowpack occurs only with the surface layer. The energy balance of the surface layer expressed in forward finite difference form over the model time step ($\Delta t$) is

$$W^{t+\Delta t} T_s^{t+\Delta t} - W^t T_s^t = \frac{\Delta t}{\rho_w c_s} (Q_r + Q_s + Q_e + Q_p + Q_m) \quad (2.18)$$

where $c_s$ is the specific heat of ice, $\rho_w$ is the density of water, $W$ is the water equivalent of the snowpack surface layer, $T_s$ is the temperature of the surface layer, $Q_r$ is the net radiation flux, $Q_s$ is the sensible heat flux, $Q_e$ is the latent heat flux, $Q_p$ is the energy flux given to the snowpack via rain or snow, and $Q_m$ is the energy flux given to the pack due to liquid water refreezing or taken from the pack during melt. Energy fluxes into the surface layer are defined as positive. If the flux terms are expressed in watts per square meter then $W$ is given in meters.

Net radiation at the snow surface ($Q_r$) is calculated through Eq. (2.17) with $T_u = T_s$ and $\alpha_u = \alpha_s$, the snow surface albedo. The snow

surface albedo is assumed to decay with age following the functional form described by Laramie and Schaake (1972)

$$\begin{aligned} \alpha_s &= 0.85(\lambda_a)^{N^{0.58}} \qquad (\textit{accumulation season}) \\ \alpha_s &= 0.85(\lambda_m)^{N^{0.46}} \qquad (\textit{melt season}) \end{aligned} \tag{2.19}$$

where $N$ is the time in days since the last snow. Based on the measurements of Storck (2000), $\lambda_a$ is 0.92 and $\lambda_m$ is 0.70 (versus 0.94 and 0.82, respectively, in the original formulation of Laramie and Schaake, 1972).

The flux of sensible heat to the snow surface is given by:

$$Q_s = \frac{\rho c_p (T_a - T_s)}{r_{as}} \tag{2.20}$$

where $r_{as}$ is the aerodynamic resistance between the snow surface and the near-surface reference height calculated through Eq. (2.8) with $d_u$ and $z_{0u}$ equal to the snow depth and roughness, respectively. Similarly, the flux of latent heat to the snow surface is given by:

$$Q_e = \frac{\lambda_i \rho \left[\frac{0.622}{P_a}\right]\left[e(T_a) - e_s(T_s)\right]}{r_{as}} \tag{2.21}$$

where $\lambda_i$ is the latent heat of vaporization when liquid water is present in the surface layer and the latent heat of sublimation in the absence of liquid water, and $P_a$ is atmospheric pressure.

Advected energy to the snowpack via the input of water is given by

$$Q_p = \frac{\rho_w c_w T_a P_L + \rho_w c_s T_a P_I}{\Delta t} \tag{2.22}$$

where $c_w$ is the specific heat of water, $P_L$ is depth of water in the liquid phase and $P_I$ is the (liquid) water equivalent of the solid phase.

The total energy available for refreezing liquid water or melting the snowpack over a given time step depends on the net energy exchange at the snow surface ($Q_{net}$):

$$Q_{net} = (Q_r + Q_s + Q_e + Q_p)\Delta t \tag{2.23}$$

If $Q_{net}$ is negative, then energy is being lost by the pack and liquid water (if present) is refrozen. If $Q_{net}$ is sufficiently negative to refreeze all liquid water, then the pack may cool. If $Q_{net}$ is positive, then the excess energy available after the cold content has been satisfied produces snowmelt.

$$\begin{aligned} Q_m\Delta t &= \min(-Q_{net}, \rho_w \lambda_f W_{liq}), \quad Q_{net} < 0 \\ Q_m\Delta t &= -(Qnet + c_s W_{ice} T_s^t), \quad Q_{net} \geq 0 \end{aligned} \tag{2.24}$$

The mass balance of the surface layer is given by

$$\begin{aligned} \Delta W_{liq} &= P_L + \left[\frac{Q_e}{\rho_w \lambda_v} - \frac{Q_m}{\rho_w \lambda_f}\right]\Delta t \\ \Delta W_{ice} &= P_I + \left[\frac{Q_e}{\rho_w \lambda_s} + \frac{Q_m}{\rho_w \lambda_f}\right]\Delta t \end{aligned} \tag{2.25}$$

where $\lambda_s$, $\lambda_v$, $\lambda_f$ are the latent heat of sublimation, vaporization, and fusion, respectively. If liquid water is present (i.e. $W_{liq} > 0$), $Q_e$ exchanges water with the liquid phase, otherwise $Q_e$ exchanges water with the ice phase.

Energy and mass exchange between the surface layer and the pack layer occurs only via the exchange of ice and from melt water which percolates from the surface layer into the pack layer. Energy exchange via conduction and diffusion between the lower layer and the surface layer and soil are ignored. If $W_{ice}$ exceeds the maximum thickness of the surface layer (typically taken as 0.10 m of SWE), then the excess, along with its cold content, is distributed to the pack layer. If $W_{liq}$ exceeds the liquid water holding capacity of the surface layer, then excess is drained to the pack layer. If the temperature of the pack layer is below freezing then liquid water transferred from the surface layer can refreeze,

warming the pack layer. Any liquid water remaining in the pack above its liquid water holding capacity is immediately routed to the soil as snowpack outflow.

### 2.4.2. Atmospheric Stability

In the presence of a snow cover, aerodynamic resistance is corrected for atmospheric stability according to the bulk Richardson's number ($Ri_b$). The Richardson's number is a dimensionless ratio relating the buoyant and mechanical forces (i.e. turbulent eddies) acting on a parcel of air (see e.g. Anderson 1976)

$$Ri_b = \frac{2gz_a(T_a - T_s)}{U(z_a)^2(T_a + T_s)} \tag{2.26}$$

with corrections for stable and unstable conditions given as

$$\begin{aligned} r_{as} &= \frac{r_{as}}{(1 - \frac{Ri_b}{Ri_{cr}})^2} && 0 \le Ri_b < Ri_{cr} \quad \textit{(stable)} \\ r_{as} &= \frac{r_{as}}{(1 - 16Ri_b)^{0.5}} && Ri_b < 0 \quad \textit{(unstable)} \end{aligned} \tag{2.27}$$

where $Ri_{cr}$ is the critical value of the Richardson's number (commonly taken as 0.2). Mixing length theory is used to place an upper limit on the bulk Richardson's number (Storck, 2000) such that $Ri_b \le [\ln(z_a/z_0) + 5]^{-1}$.

## 2.5. CANOPY SNOW INTERCEPTION AND RELEASE

The canopy snow model described by Storck and Lettenmaier (1999) and Storck (2000) is used to represent explicitly the combined canopy processes that govern snow interception, sublimation, mass release, and melt from the forest canopy. Atmospheric precipitation ($P$) is partitioned into snowfall and rainfall via:

$$
\begin{aligned}
P_s &= P, && T_a \le T_{min} \\
P_s &= \frac{T_{max} - T_a}{T_{max} - T_{min}} P, && T_{min} < T_a < T_{max} \\
P_s &= 0, && T_a \ge T_{max} \\
P_r &= P - P_s
\end{aligned}
\tag{2.28}
$$

where $P_r$ is depth of rainfall, $P_s$ is the water equivalent of snowfall, $T_{\min}$ is a threshold temperature below which all precipitation is in the form of snow, and $T_{\max}$ is a threshold temperature above which all precipitation is rain. Between the threshold temperatures precipitation is assumed to be a mix of rain and snow.

### 2.5.1. Snow Interception

During each time step, snowfall is intercepted by the overstory up to the maximum interception storage capacity according to

$$I = f\ P_s \tag{2.29}$$

where $I$ is the water equivalent of snow intercepted during a time step, $f$ is the efficiency of snow interception, and $P_s$ is snowfall over the time step given by Eq. (2.2). The maximum interception capacity ($B$) is given by

$$B = L_r(r_m LAI_o) \tag{2.30}$$

where $r_m$ is determined based on observations of maximum snow interception capacity. The leaf area ratio ($L_r$) is a step function of temperature:

$$
\begin{aligned}
L_r &= 0.004 && T_a > -5^0C \\
L_r &= 0.001 && T_a \le -5^0C
\end{aligned}
\tag{2.31}
$$

This step function is based on observations from previous studies of intercepted snow as well as data collected by Storck (2000). Newly intercepted rain is calculated with respect to the water holding capacity

of the intercepted snow ($W_c$), which is given by the sum of the capacity of the snow and the bare branches:

$$W_c = hW_{ice} + 1e^{-4}(LAI_2) \tag{2.32}$$

where $h$ is the water holding capacity of snow (taken as 0.035) and $LAI_2$ is the all-sided leaf area index of the canopy. Excess rain becomes throughfall ($T_{co}$).

### 2.5.2. Release of Intercepted Snow

The intercepted snowpack can contain both ice and liquid water. The mass balance for each phase is:

$$\Delta W_{ice} = I - M + \left[\frac{Q_e}{\rho_w \lambda_s} + \frac{Q_m}{\rho_w \lambda_f}\right]\Delta t \tag{2.33}$$

$$\Delta W_{liq} = P_r + \left[\frac{Q_e}{\rho_w \lambda_v} - \frac{Q_m}{\rho_w \lambda_f}\right]\Delta t \tag{2.34}$$

where $M$ is snow mass release from the canopy. Snowmelt is calculated directly from a modified energy balance, similar to that applied for the ground snowpack, in which

$$T_s = \min(T_a, 0) \tag{2.35}$$

Testing of a fully iterative (on $T_s$) intercepted snow energy balance revealed that the intercepted snow temperature closely followed that predicted by Eq. (2.35).

Given the intercepted snow temperature and air temperature, snowmelt is calculated directly from Eq. (2.34) and Eq. (2.35). The individual terms of the energy balance are as described for the ground snowpack model (section 2.4). However, the aerodynamic resistance is calculated via Eq. (2.7) and the shortwave and longwave radiation balance from Eq. (2.15). Snowmelt in excess of the liquid water holding capacity of the snow ($W_c$) results in meltwater drip ($D_r$). Mass release

of snow from the canopy occurs if sufficient snow is available and is related linearly to the production of meltwater drip:

$$\begin{aligned} M &= 0 \qquad & W_{ice} \le n \\ M &= 0.4D_r \qquad & W_{ice} > n \end{aligned} \tag{2.36}$$

where $n$ is the residual intercepted snow that can only be melted (or sublimated) off the canopy (taken as 5 mm based on observations of Storck, 2000). The ratio of 0.4 in Eq. (2.36) is derived from observations of the ratio of mass release to meltwater drip as discussed in Storck, 2000.

Rainfall and snowfall not intercepted by the canopy combine with mass release and drip to contribute energy and mass to the ground snowpack through Eq. (2.22) and Eq. (2.11). The depth of liquid delivered to the ground snowpack ($P_L$) is equal to

$$P_L = P_r(1 - F) + T_{co} + D_r \tag{2.37}$$

The (liquid) water equivalent depth of solid phase ($P_I$) is given by

$$P_I = P_s(1 - f)F + P_s(1 - F) + M \tag{2.38}$$

## 2.6. UNSATURATED SOIL MOISTURE MOVEMENT

The soil surface may receive water from throughfall, snowmelt, or surface runoff from adjacent cells (sections 2.3, 2.4, and 2.8, respectively). A user defined maximum infiltration rate determines the total depth of water that can be infiltrated during the time step. Any excess water is available for surface routing. Unsaturated moisture movement is simulated using a multi-layer representation based on the two-soil layer model of Wigmosta et al. (1994). Each vegetation layer may remove water from one or more soil layers, and each soil layer may contain roots from one or more vegetation layers. Transpiration by a given canopy is first calculated for each soil layer using Eq. (2.2), then multiplied by the root fraction in that soil layer. Soil evaporation is restricted to the upper zone.

Mass balance equations for the upper soil layer, intermediate layers, and the lower layer are

$$d_1\left(\theta_1^{t+\Delta t} - \theta_1^t\right) = I_f - Q_v\left(\theta_1\right) - \sum_{j=1}^{2} f_{rj1} E_{tj} - E_s + V_{ex2} - V_{ex1} \quad (2.39)$$

$$d_k\left(\theta_k^{t+\Delta t} - \theta_k^t\right) = Q_v\left(\theta_{k-1}\right) - Q_v\left(\theta_k\right) - \sum_{j=1}^{2} f_{rjk} E_{tj} + V_{exk+1} \quad (2.40)$$

$$d_{ns}\left(\theta_k^{t+\Delta t} - \theta_k^t\right) = Q_v\left(\theta_{ns-1}\right) + \left(Q_{Sin}^t - Q_S^t\right)\Delta t \quad (2.41)$$

where $d_k$ is the soil layer thickness, $\theta_k$ is the average soil moisture, $I_f$ is the volume of water infiltrated during the time step, $Q_v$ is the volume of water discharged downward to the next layer, $f_{rjk}$ is the fraction of roots from vegetation layer $j$ in soil layer $k$, $V_{exk}$ is the volume of water supplied by a rising water table, $E_s$ is the volume of evaporated soil moisture from the surface layer, and $Q_{Sin}^t$ and $Q_S^t$ are the volumes of lateral subsurface inflow and outflow at the start of the time step, respectively (see section 2.7). The model first calculates infiltration into the upper layer, then downward vertical moisture transfer ($Q_v$'s) moving from top to bottom. The net flux of lateral saturated subsurface flow ($Q_{Sin} - Q_S$) is the added to the bottom soil layer and soil moisture is updated for each layer ($\theta_k^{t+\Delta t}$). Starting at the bottom, each layer is then checked to determine if the recalculated soil moisture is greater than the porosity ($\theta_k^{t+\Delta t} > \phi_k$). If so, $V_{exk} = \theta_k^{t+\Delta t} - \phi_k$ and the soil moisture is set equal to the porosity, otherwise $V_{exk} = 0$. $V_{exk}$ is then added to the overlying layer and the process is continued layer-by-layer to the surface. Any excess water in the surface layer ($V_{ex1}$) represents the return of subsurface water to the surface and is available for overland flow routing (section 2.8).

In earlier versions of the model the vertical depth to the water table ($z$) was taken as the distance from the soil surface to the top of the uppermost saturated soil layer. This could result in rapid fluctuations of the water table when a layer first became saturated or "unsaturated" and the water table jumped by the thickness of the layer. To smooth this response, $z$ is now given as

$$z = D\left[1 - \sum_{k=1}^{ns}\left(\theta_k^{t+\Delta t} - \theta_{fck}\right)d_k \Big/ \sum_{k=1}^{ns}\left(\phi_k - \theta_{fck}\right)d_k\right] \quad (2.42)$$

where $ns$ is the number of soil layers, and $\theta_{fck}$ is the soil field capacity for layer $k$.

### 2.6.1. Percolation

The rate of downward unsaturated moisture movement $(q_v)$ is calculated via Darcy's Law assuming a unit hydraulic gradient with the Brooks-Corey equation used to calculate hydraulic conductivity

$$q_v(\theta) = K_s\left[\frac{\theta - \theta_r}{\phi - \theta_r}\right]^{(2/m)+3} \tag{2.43}$$

where $K_s$ is the soil vertical saturated hydraulic conductivity, $m$ is the pore size distribution index, $\phi$ is the soil porosity, and $\theta_r$ is the residual soil moisture content. For simplicity, the saturated moisture content $\theta_s$ is taken equal to $\phi$ (i.e., $\theta_r = 0$). The discharge volume over the time step is given as (Wigmosta et al., 1994)

$$Q_{vk} = \tfrac{1}{2}\left[q_v\left(\theta_k^t\right) + q_v\left(\hat{\theta}\right)\right]\Delta t \tag{2.44}$$

where $\hat{\theta}$ is an updated moisture content that includes input from the overlying layer given by $\hat{\theta} = \theta_k^t + Q_{vk-1}^{t+\Delta t}/D_k$ .

### 2.6.2. Desorption

Soil water evaporation from the upper soil layer, $E_s$, is given by Eq. (2.6) as a function of the potential evaporation demand at the soil surface ($E_{ps}$) and ($F_e$), the soil desorptivity. Desorption is calculated based on the work of Eagleson (1978) and Entekhabi and Eagleson (1989) (see Wigmosta et al. (1994) for details)

$$F_e = S_e \Delta t^{1/2} \tag{2.45}$$

Sorptivity ($S_e$) is calculated using the method presented by Entekhabi and Eagleson (1989)

$$S_e = \left[\frac{8\phi K_s \Psi_b}{3(1+3m)(1+4m)}\right]^{1/2}\left[\frac{\theta}{\phi}\right]^{(1/2m+2)} \tag{2.46}$$

where $\Psi_b$ is the soil bubbling pressure. Following the approach of Entekhabi and Eagleson (1989), the soil moisture content is assumed to be uniform at the beginning of a time step (i.e., unit gradient assumption with $\theta$ given by Eq. (2.39)) and $t$ in Eq. (2.45) is reset to zero.

## 2.7. SATURATED SUBSURFACE FLOW

DHSVM employs a cell-by-cell approach to route saturated subsurface flow (Wigmosta et al., 1994; Wigmosta and Lettenmaier, 1999) using either a kinematic or diffusion approximation. Model grid cells are centered on each DEM elevation point (Fig. 2.1). Directions between a node and its neighbors are assigned the index $k$ and numbered from 0 to 7 in a clockwise direction from north. On steep slopes with thin, permeable soils, hydraulic gradients may be approximated by local ground surface slopes (kinematic assumption). In areas of low relief, hydraulic gradients must be approximated by local water table slopes (diffusion assumption).

The rate of saturated subsurface flow from cell $i, j$ in the $k$-direction ($q_{Si,j,k}$) is given by:

$$q_{Si,j,k} = w_{i,j,k}\,\beta_{i,j,k}\;T_{i,j}(z,D) \tag{2.47}$$

where $w_{i,j,k}$ is the grid cell flow width in the $k$-direction, $\beta_{i,j,k}$ is the water table slope in the $k$ direction, and $T_{i,j}(z,D)$ is the grid cell transmissivity. Soil lateral saturated hydraulic conductivity is assumed to decrease exponentially with depth, allowing soil transmissivity in Eq. (2.47) to be calculated as:

$$T_{i,j}(z,D) = \frac{K_{i,j}}{f_{i,j}}\left(e^{-f_{i,j}z_{i,j}} - e^{-f_{i,j}D_{i,j}}\right) \tag{2.48}$$

where $K_{i,j}$ is the grid cell lateral saturated hydraulic conductivity at the soil surface, $f_{i,j}$ is a decay coefficient, and $D_{i,j}$ is the grid cell soil

thickness. The total subsurface outflow from a grid cell $Q_{S_{i,j}}$ is equal to the sum of the component flows by Eq. (2.47).

### 2.7.1. Interception by Roads and Channels

As subsurface water moves downslope toward a stream channel it may be intercepted by the road network. This occurs in grid cells containing a road, when the depth to the water table ($z$) is less than the depth of the road cut ($z_R$). Saturated subsurface flow is intercepted by the road at a rate given by (Wigmosta and Perkins, 2001):

$$Q_{R_{i,j}} = w_{R_{i,j}} \beta_{i,j} T_{i,j}(z, z_R) \tag{2.49}$$

where $w_{R_{i,j}}$ is the straight-line length of road in the grid cell orthogonal to the cell aspect $\alpha_{i,j}$, $\beta_{i,j}$ is the grid cell slope corresponding to $\alpha_{i,j}$, and $T_{i,j}(z, z_R)$ is the transmissivity of the saturated zone above the road-cut, obtained by substituting $z_R$ for $D$ in Eq. (2.48). The total flux of subsurface flow that continues to pass beneath the road ($Q_{S_{i,j}}$) is obtained using $z_R$ in place of $z$ in Eq. (2.47) and Eq. (2.48).

A grid cell will contribute water to a stream reach when the grid cell water table rises above the streambed (Fig. 2.2). Subsurface flow will be intercepted by the channel at a rate given by (Wigmosta and Perkins, 2001):

$$Q_{C_{i,j}} = 2L_{C_{i,j}} \beta_{C_{i,j}} T_{i,j}(z, z_C) \tag{2.50}$$

where is $z_C$ is the depth to the channel bed, $L_{C_{i,j}}$ is the length of channel crossing the grid cell, and $T_{i,j}(z, z_C)$ is the transmissivity of the saturated zone above the streambed, obtained by substituting $z_C$ for $D$ in Eq. (2.48). The hydraulic gradient is approximated by:

$$\beta_{Ci,j} = \frac{z_{C_{i,j}} - z_{i,j}}{0.5 w_{C_{i,j}}} \tag{2.51}$$

where $w_{C_{i,j}}$ is the width of the stream reach. If surface water is available within the cell, it is contributed to the stream reach in the same time interval.

## 2.8. OVERLAND FLOW

Surface runoff is generated in a grid cell when: 1) the input of throughfall and snowmelt, exceeds the user defined infiltration capacity (infiltration excess runoff); 2) throughfall or snowmelt occurs on a saturated cell (saturation excess runoff); or 3) the water table rises above the ground surface (return flow). Two methods are available for routing surface runoff, an explicit cell-by-cell approach or a unit hydrograph approach. The explicit method must be used if the model application contains roads or channels.

The downslope movement of surface runoff is done on a cell-by-cell basis similar to the method used for subsurface flow. Outflow in the *k*-direction ($q_{O_{i,j,k}}$) is given by (Wigmosta and Perkins, 2001):

$$q_{o_{i,j,k}} = w_{i,j,k}\, v_{i,j}\, y_{i,j} \tag{2.52}$$

where $v_{i,j}$ is the grid cell flow velocity, $y_{i,j}$ is the grid cell flow depth, and $w_{i,j,k}$ as defined in Eq. (2.47). The total outflow ($Q_{O_{i,j}}$) is the sum of component flows from Eq. (2.52). The surface water volume at the end of the time step ($S_O^{t+\Delta t}$) is given by:

$$S_{O_{i,j}}^{t+\Delta t} = S_{O_{i,j}}^{t} + V_{ex1_{i,j}} + I_{ex_{i,j}} + \left( Q_{Oin_{i,j}} + Q_{cvrt_{i,j}} - Q_{O_{i,j}} \right) \Delta t \tag{2.53}$$

where $Q_{o_{in_{i,j}}}$ is the total amount of overland flow into cell *i, j* from up-gradient cells, $I_{ex_{i,j}}$ is the volume of infiltration excess runoff, and $Q_{cvrt_{i,j}}$ is culvert outflow. The model currently uses a constant velocity of $v = \Delta x / \Delta t$, where $\Delta x$ is the grid cell width. This implies that the volume of overland flow leaving a grid cell over the time step is equal to the surface water storage at the start of the time step.

In the unit hydrograph approach, the time required for surface runoff generated at a given cell to travel to the basin outlet is calculated for each cell. The response function from each cell is a function of this travel time and can consist of both a linear translation component and a linear storage component. The routing model was developed by Maidment et al. (1994) and its incorporation in DHSVM is described in detail by Storck et al. (1995).

## 2.9. CHANNEL FLOW

Flow in road drainage ditches and stream channels is routed using a cascade of linear channel reservoirs. The stream and road channel networks comprise of any number of individual segments, each of which will have its own hydraulic parameters. Lateral inflow to a channel segment, from the watershed cells through which it passes, consists of overland flow ($Q_o$ via Eq. (2.52)) and subsurface flow intercepted by roads ($Q_R$ via Eq. (2.49)) or channels ($Q_C$ via Eq. (2.50)). Outflow from a segment may drain to another segment or exit the watershed. Outflow from a road channel segment may also be input back into a watershed cell at culvert locations. In which case, the outflow from the channel segment is added to the surface water of the cell, making it available for reinfiltration and overland flow routing through Eq. (2.52).

A relatively simple, robust linear storage routing algorithm is available for channel routing. Each channel reach is treated as a reservoir of constant width with outflow linearly related to storage ($V_c$). The linear storage-discharge relationship implies a constant flow velocity that is calculated from Manning's equation using a reference flow depth and corresponding hydraulic radius, allowing the storage at time $t+1$ to be calculated as (Wigmosta and Perkins, 2001)

$$V_c^{t+1} = \frac{Q_{in}}{k} + \left( V_c^t - \frac{Q_{in}}{k} \right) \exp(-k\Delta t) \tag{2.54}$$

where $Q_{in}$ is the average rate of lateral and upstream inflow to the reach during the time step, and $k$ is the reach storage parameter given by

$$k = \frac{R_r^{2/3}\sqrt{S_o}}{n\Delta L} \tag{2.55}$$

where $R_r$ is the hydraulic radius at the reference flow depth, $S_o$, $\Delta L$, and $n$ are the channel slope, length, and hydraulic roughness, respectively. The average outflow from the reach is obtained through mass balance; i.e., $Q_{out} = Q_{in} - (V_c^{t+1} - V_c^t) / \Delta t$.

A Muskingum-Cunge method is also available (Garbrecht and Brunner, 1991; Chow et al., 1998) for channel routing (see Wigmosta and Perkins, (2001) for complete details). In some situations the

Muskingum-Cunge method exhibited problems with stability, which lead to incorporation of the linear storage model. The linear storage algorithm has provided satisfactory results when applied to a large range of basin sizes and topographic characteristics making it the method of routing used in most current applications of DHSVM.

## 2.10. MODEL EVALUATION AND APPLICATIONS

During the last several years DHSVM has been applied to a range of research activities and most components of the model have been tested against field measurements. We present three brief examples to illustrate the types of research activities that were involved. The first is an evaluation of the model's ability to simulate mass and energy fluxes under snow free conditions. The second tests the model's representation of snow processes, while the third considers the impacts of logging roads on soil water redistribution and streamflow.

### 2.10.1. Evaluation of Mass and Energy Fluxes under Snow Free Conditions

Surface mass and energy balance components of the model were evaluated by Nijssen et al. (1997) using flux tower measurements collected as part of the Boreal Ecosystem Atmosphere Study (BOREAS). Model simulated net radiation, latent heat flux, and sensible heat flux are compared with observations in Fig. 2.3. Net radiation was simulated through Eq. (2.15) and Eq. (2.17); the latent heat flux is given by $\lambda_v E_T$ with $E_T$ calculated via Eq. (2.5); sensible heat ($H$) was found through solution of the surface energy balance equation as $H = \lambda_v E_T + G + \Delta Q_g$, where the ground heat flux ($G$) and the change in ground heat storage ($\Delta Q_g$) are computed by the model.

Model simulated net radiation and latent heat flux generally showed good agreement with measurements at two mature Black Spruce sites and one mature Jack Pine site (Fig. 2.3). A phase shift was observed in the simulated sensible heat flux. This timing problem was attributed to the soil heat algorithm, which may be too simplistic and require additional improvements.

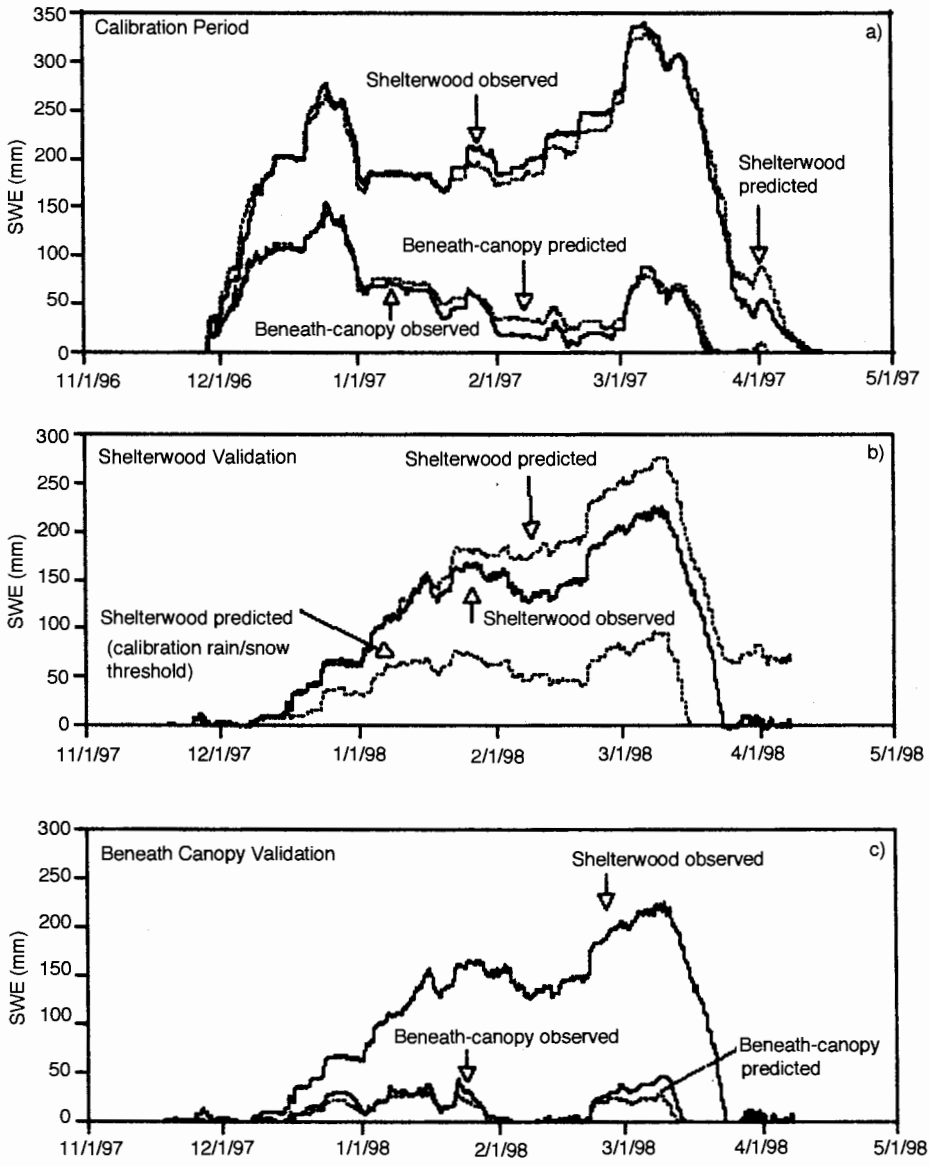


**Fig. 2.3. Observed and simulated net radiation, sensible heat flux, and latent heat flux from August 30 - September 19, 1994 for Southern Old Black Spruce measurement site, Boreal Ecosystem Atmosphere Study (BOREAS) (adapted form Nijssen et al., 1997).**

### 2.10.2. Evaluation of Canopy Snow Interception and Ground Snowpack

Performance of the canopy snow interception and ground snowpack models was evaluated against extensive field measurements in the transient snow zone (1200 m) of the Southern Oregon Cascades by Storck and Lettenmaier (1999) and Storck (2000). Annual precipitation is about 2 m and average winter temperatures are often near freezing at this location. Snow cover is generally present throughout the winter in clearings with average maximum water equivalents of about 350 mm. Mid-winter melt is common and is driven mainly by turbulent heat fluxes. The site is exposed to frequent rain-on-snow events and a pronounced radiation dominated melt season each spring. Measurements were taken with large (~25 $m^2$) weighing lysimeters below a mature forest canopy dominated by Douglas-fir (*Pseudotsuga menziesii*) and in an adjacent harvested (open) site. The mature canopy has average tree heights approaching 40 m and an average canopy closure of approximately 80 percent. Snow interception and canopy dynamics were inferred by comparing data from the two beneath-canopy lysimeters to that from the adjacent open site (Shelterwood).

The model was calibrated against the Shelterwood and beneath-canopy lysimeter data for the 1996/97 snow year (Fig. 2.4a). Accumulation and ablation of snow water equivalent (SWE) were well predicted at both sites. The model was validated against 1997/98 Shelterwood data (Fig. 2.4b). Given the calibration threshold rain-snow temperatures (-1.0, 0.5), SWE was significantly underestimated, especially during the initial accumulation phase. Adjusting the rain and snow threshold to 0.4 °C and 0.5 °C, respectively, yielded the best agreement with observations. This change also caused considerable over-prediction of late season SWE due to the continual accumulation of snow from 1-Feb 1998 to 20-Feb 1998. Ironically, the best fit for the late season snow accumulation was obtained with the original rain-snow threshold values. Given that 1997/98 was a strong El-Nino year, a time dependent rain-snow threshold may be defensible, but in the absence of observations of the form of precipitation such a time dependant threshold simply becomes an exercise in curve fitting. Therefore, the higher rain-snow threshold was adopted for the beneath-canopy simulations. Figure 2.4c shows the validation of the below canopy snow model. Given sufficient snow at the Shelterwood site, beneath-canopy

SWE accumulation and ablation were quite well predicted. Complete details are given in Storck and Lettenmaier (1999) and Storck (2000).

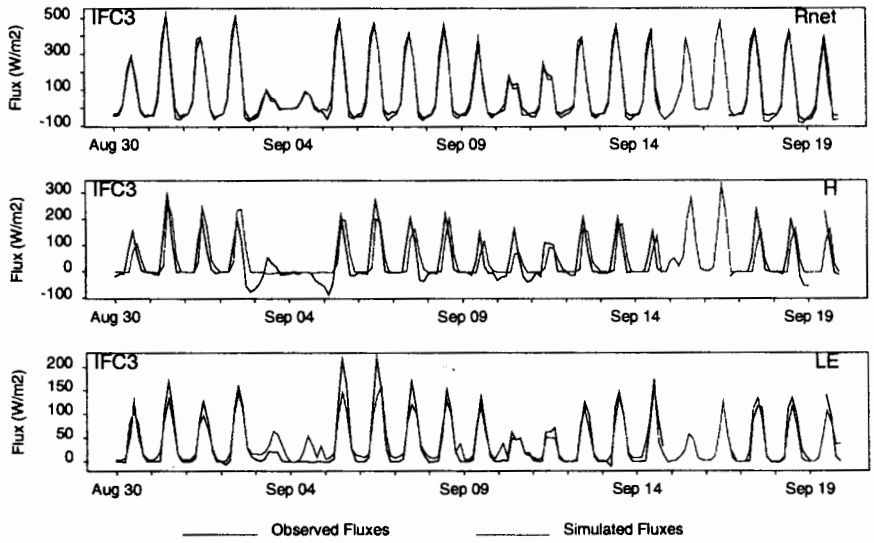


**Fig. 2.4. Results of a) full canopy snow model calibration to 1996/97 weighing lysimeter data below the mature canopy and in the adjacent open (Shelterwood) site and, b) validation against 1997/98 Shelterwood data, and c) validation against 1997/98 beneath-canopy data. Note the two predicted SWE simulations for the Shelterwood validation (b). The lower curve uses a rain/snow threshold of (-1.0, 0.5) (identical to the calibration period (a)) while the upper curve uses (0.4, 0.5). Subsequent validation against the beneath canopy data uses (0.4, 0.5) as the rain/snow threshold (adapted from Storck and Lettenmaier, 1999).**

## 2.10.3. Impacts of Flow Interception by Logging Roads

The road interception algorithms have been evaluated in studies by Lamarche and Lettenmaier (1998), Bowling and Lettenmaier (2001), and Wigmosta and Perkins (2001). Wigmosta and Perkins (2001) studied the influences of logging roads in the Carnation Creek Basin on the west coast of Vancouver Island BC, Canada. They demonstrated that even where the integrated impact of the road network produces minor

changes in streamflow at the basin outlet, subsurface flow interception by roads alters significantly the distribution of soil moisture and runoff generation in many areas of the basin (Fig. 2.5). The road network may effectively increase the contributing area of some channel segments and decrease the area draining to others. For example, stream segments 121 and 130 are adjacent to each other with natural drainage areas that are similar in size. The road that bisects the two channels captures some water that would normally flow to segment 130 and routs it to segment 121 instead. This can be seen in Fig. 2.6 which presents simulated hourly discharge for channel segments 121 and 130 without roads, with roadcut depths of 0.4 m (one-half the soil thickness) and 0.8 m (the total soil thickness). Discharge in segment 121 is increased greatly by a road network with 0.8 m cut depths. In this case the road system begins to intercept subsurface flow very early in the storm, increasing the effective contributing area (and discharge) relative to natural conditions. A road network with 0.4 m cut depths does not begin to impact channel flow until water tables rise above local road cut elevations. By the time significant flow interception occurs, the rainfall has reached its peak and decreases rapidly. As a result, the additional contributing area from the road causes a moderate increase in discharge relative to the non-road case.

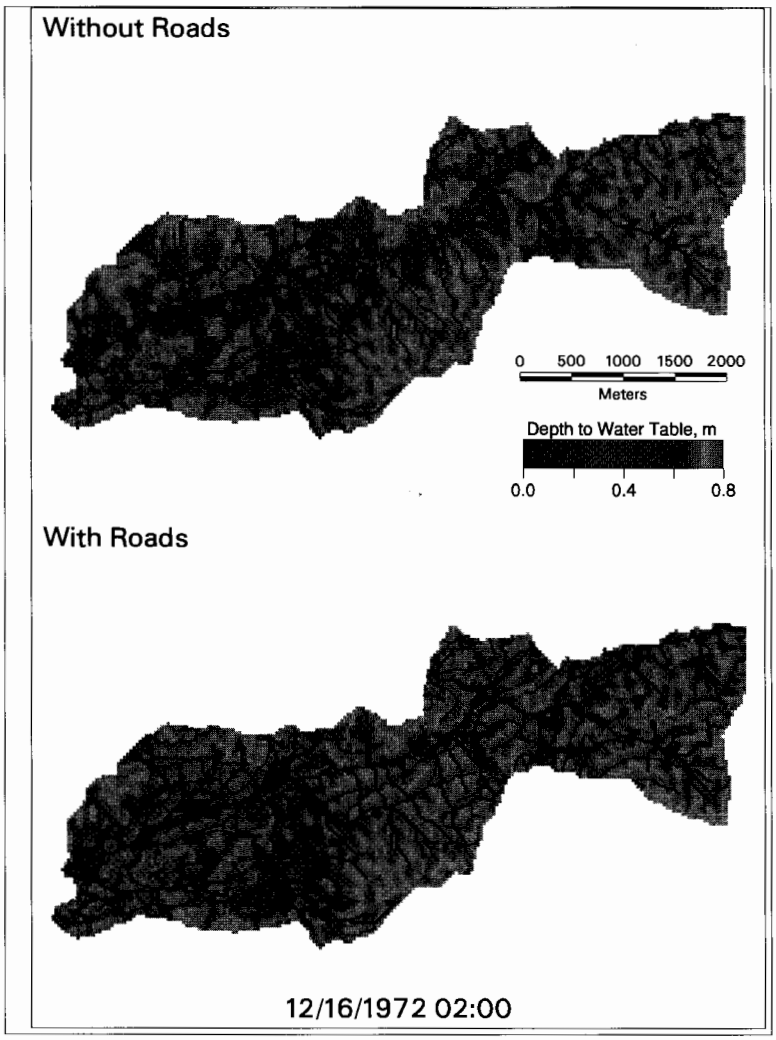


**Fig. 2.5.** **Simulated depth to the water table (m) in the Carnation Creek Basin near peak discharge on December 16, 1972 without roads (upper) and with roads (lower). The bands of lower watertables below roads result from the interception of subsurface flow by the road drainage network. Redistribution of intercepted water by the road drainage system produces significant streamflow changes in many tributaries (adapted from Perkins and Wigmosta, 2001).**

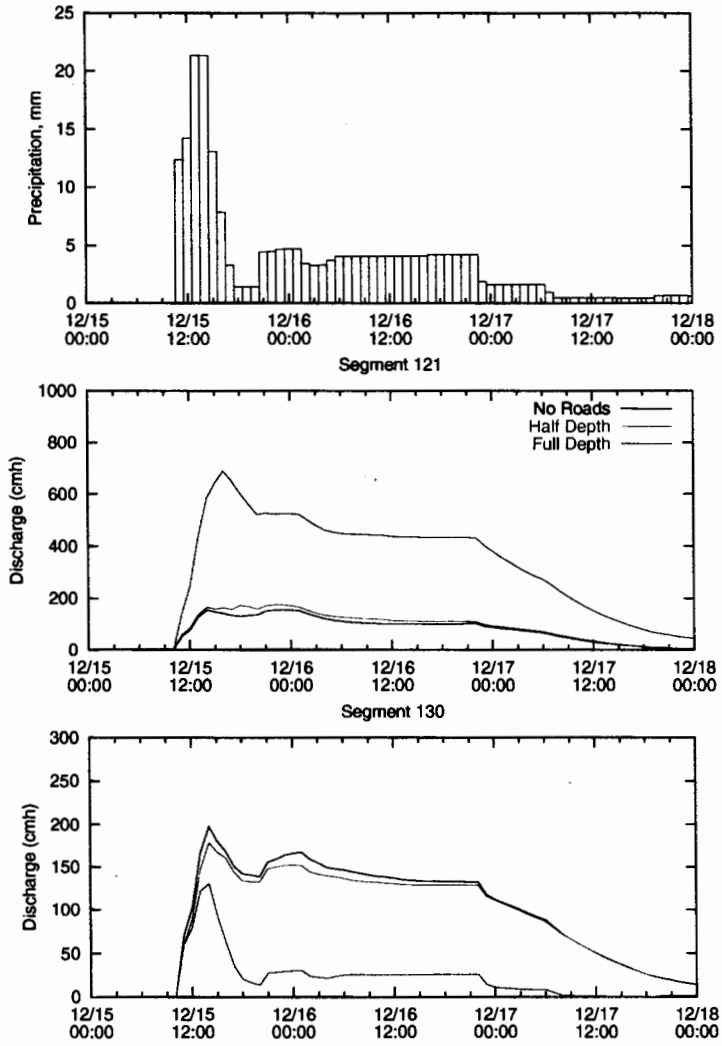


**Fig. 2.6.** **Hourly basin-averaged precipitation for December 15-17, 1972 (upper) and simulated hourly discharge ($m^3/h$) with and without roads for channel segments 121 (middle) and 130 (lower). Simulated discharge is presented without roads, with roadcut depths of 0.4 m (one-half the soil thickness), and roadcut depths of 0.8 m (the total soil thickness) (adapted from Perkins and Wigmosta, 2001).**

Channel segment 130 provides an example where the road network diverts water away from the channel, reducing streamflow. In the first two hours of the storm (up to a discharge of ~ 70 $m^3/h$) discharge is the same in all three scenarios because the area contributing directly to the channel has not extended upslope to the road system. With a 0.8 m cut depth the channel contributing area can not extend above the road locations, resulting in lower discharges than under natural conditions. The 0.4-m cut depth results in flows close to, but lower than the non-road case.

## SUMMARY AND CONCLUSIONS

We have described the current state of the Distributed Hydrology Soil Vegetation Model (DHSVM) along with results from field tests and applications. The model provides an integrated representation of watershed processes at the spatial scale described by DEM data. Canopy snow interception and release are modeled using a single-layer mass- and energy-balance model. Snow accumulation and melt below the canopy are simulated using a two-layer mass- and energy-balance model that explicitly incorporates the effects of topography and vegetation cover on the energy and mass exchange at the snow surface. Evapotranspiration is represented using a two-layer canopy model with each layer partitioned into wet and dry areas. Unsaturated moisture movement through multiple rooting zone soil layers is calculated using Darcy's Law. Cell-by-cell routing produces three-dimensional representations of surface and saturated subsurface flow. Flow in road drainage ditches and stream channels is routed using a cascade of linear channel reservoirs.

Three examples were used to illustrate the types of research activities that utilize DHSVM. Surface mass and energy balance components of the model were evaluated using flux tower measurements from BOREAS. Model simulated net radiation and latent heat flux generally showed good agreement with measurements. A phase shift was observed in the simulated sensible heat flux, likely the result of a soil heat algorithm that requires additional improvements. Performance of the canopy snow interception and ground snowpack models was evaluated using field measurements in the transient snow zone of the Southern Oregon Cascades. During calibration,

accumulation and ablation of snow water equivalent (SWE) was well predicted in the open and under a mature forest canopy. Although SWE was significantly underestimated in the open site during validation, beneath-canopy SWE accumulation and ablation were quite well predicted. The model was also used to study the influences of logging roads in an experimental watershed on the west coast of Vancouver Island BC, Canada. It was demonstrated that even where the integrated impact of the road network produces minor changes in streamflow at the basin outlet, subsurface flow interception by roads alters significantly the distribution of soil moisture and runoff generation in many areas of the basin. The impact of road network on tributary streamflows was shown to vary during a storm based on the road design, storm characteristics, and topography.

## REFERENCES

Anderson, E. A., A point energy and mass balance model of snow cover, *NWS Technical Report 19*, National Oceanic and Atmospheric Administration, Washington, D.C., 150p., 1976.

Arola, A., and D. P. Lettenmaier, Effects of subgrid spatial heterogeneity on GCM-scale land surface energy and moisture fluxes, *J. Climate*, 9, 1339-1349, 1996.

Bowling, L., P. Storck, and D. P. Lettenmaier, Hydrologic effects of logging in Western Washington, *Water Resources Research*, in review, 2000.

Bowling, L., and D. P. Lettenmaier, The effects of forest roads and harvest on catchment hydrology in a mountainous maritime environment, in *Influence of Urban and Forest Land Use on the Hydrologic-Geomorphic Responses of Watersheds*, M.S. Wigmosta and S.J. Burges, eds., AGU Water Science and Applications Series, 2, in press, 2001.

Chow, V.T., D.R. Maidment, and L.W. Mays, *Applied Hydrology*, McGraw-Hill, Inc., New York, 572p., 1988.

Deardorff, J. Efficient prediction of ground temperature and moisture with inclusion of a layer of vegetation, *J. Geophysical Research*, 83, 1889-1903, 1978.

Dickinson, R. E., A. Henderson-Sellers, C. Rosenzweig, and P. J. Sellers, Evapotranspiration models with canopy resistance for use in climate models, a review, *Agric. For. Meteorol.*, 54, 373-388, 1991.

Dickinson, R. E., A. Henderson-Sellers, P. J. Kennedy, and M. F. Wilson, Biosphere-atmosphere transfer scheme (BATS) for the NCAR Community Climate Model, *NCAR Technical Note, NCAR/TN-275+STR*, Boulder, Colorado, 1986.

Dickinson, R. E., A. Henderson-Sellers, and P. J. Kennedy, Biosphere-atmosphere transfer scheme (BATS) Version 1e as coupled to the NCAR Community Climate Model, *NCAR Technical Note, NCAR/TN-387+STR*, Boulder, Colorado, 1993.

Eagleson, P. S., Climate, soil, and vegetation 3. A simplified model of soil moisture movement in the liquid phase, *Water Resources Research*, 14(5), 722-730, 1978.

Entekhabi, D., and P. S. Eagleson, Land surface hydrology parameterization for atmospheric general circulation models: inclusion of subgrid scale spatial variability and screening with a simple climate model, *Ralph M. Parsons Laboratory Report No. 325*, Massachusetts Institute of Technology, 195p., 1989.

Feddes, R. A., P. J. Kowalik, and H. Zaradny, *Simulation of field water use and crop yield*, John Wiley and Sons, New York, 188 pp., 1978.

Garbrecht, J., and G. W. Brunner, A Muskingum-Cunge channel flow routing method for drainage networks, *J. Hydraulic Engineering, ASCE, 117 (5)*, 629-642, 1991.

Haddeland, I., and D.P. Lettenmaier, Hydrologic modeling of boreal forest ecosystems, *Water Resource Series, Technical Report 145*, Dept. of Civil Engineering, University of Washington, 1995.

Kenward, T., and D. P. Lettenmaier, Assessment of required accuracy of digital elevation data for hydrologic modeling, *Water Resource Series, Technical Report 153*, Dept. of Civil Engineering, University of Washington, 1997.

Lamarche, J., and D. P. Lettenmaier, Forest road effects on flood flows in the Deschutes river basin, Washington, *Water Resource Series, Technical Report,* Dept. of Civil Engineering, University of Washington, 1998.

Laramie, R. L., and J. C. Schaake, Jr., Simulation of the continuous snowmelt process, Ralph M. Parsons Laboratory Report No. 143, Massachusetts Institute of Technology, 1972.

Leung, L.R., M.S. Wigmosta, S.J. Ghan, D.J. Epstein, and L.W. Vail, Application of a subgrid orographic precipitation/surface hydrology scheme to a mountain watershed, *J. Geophysical Research*, 101 (D8), 12,803-12,817, 1996.

Leung, L.R., and M.S. Wigmosta, Potential climate change impacts on mountain watersheds in the Pacific Northwest, J. Amer. Water Resour. Assoc., 35 (6), 1463-1471, 1999.

Maidment, D. R., J. F. Olivera, A. Calver, A. Eatherall, and W. Fraczeck, A unit hydrograph derived from a spatially distributed velocity field, Hydrologic Processes, 10, 1996.

Monteith, J. L. and M. H. Unsworth, *Principles of environmental physics*, Routledge, Chapman and Hall, New York, NY, 291 pp., 1990.

Nijssen, B., I. Haddeland, and D. P. Lettenmaier, Point evaluation of a surface hydrology model for BOREAS, *J. Geophysical Research*, 102, 29,367-29,378, 1997.

Storck, P., D. P. Lettenmaier, B. A. Connelly, and T. W. Cundy, Implications of forest practices on downstream flooding: Phase II Final Report, Washington Forest Protection Association, TFW-SH20-96-001, 1995.

Storck, P., L. Bowling, P. Wetherbee, and D. P. Lettenmaier, An application of a GIS-based distributed hydrology model for the prediction of forest harvest effects on peak streamflow in the Pacific Northwest, *Hydrologic Processes*, (12), 889-904, 1998.

Storck, P., T. Kern, and S. Bolton, Measurement of differences in snow accumulation, melt and micrometeorology due to forest harvesting, *Northwest Science*, (73), 87-100, 1999.

Storck, P., and D. P. Lettenmaier, Predicting the effect of a forest canopy on ground snow accumulation and ablation in maritime climates, in Troendle, C, Ed., *Proc. 67th Western Snow Conf.*, Colorado State University, Fort Collins, 1-12, 1999.

Storck, P., Trees, snow and flooding: an investigation of forest canopy effects on snow accumulation and melt at the plot and watershed scales in the Pacific Northwest, *Water Resource Series, Technical Report 161*, Dept. of Civil Engineering, University of Washington, 2000.

Westrick, K. J., C. F. Mass, B. Nijssen, D. McDonnal, P. Storck, and D. P. Lettenmaier, Description of a high resolution hydrometeorological forecast system configured for real-time application, Weather *Analysis and Forecasting*, in review, 2000.

Wigmosta, M.S., L. W. Vail, and D. P. Lettenmaier, A distributed hydrology-vegetation model for complex terrain, *Water Resources Research*, 30 (6), 1665-1679, 1994.

Wigmosta, M.S., L.R. Leung, and E. Rykiel, Regional modeling of climate-terrestrial ecosystems interactions, *J. Biogeography*, (22), 453-465, 1995.

Wigmosta, M.S., and D.P. Lettenmaier, A comparison of simplified methods for routing topographically-driven subsurface flow, *Water Resources Research*, 35 (1), 255-264, 1999.

Wigmosta, M.S. and W.A. Perkins, Simulating the effects of forest roads on watershed hydrology, in *Influence of Urban and Forest Land Use on the Hydrologic-Geomorphic Responses of Watersheds*, M.S. Wigmosta and S.J. Burges, eds., AGU Water Science and Applications Series, 2, in press, 2001.

Wigmosta, M.S. and L.R. Leung, Potential impacts of climate change on streamflow and flooding in forested basins, in *The influence of Environmental Change on Geomorphological Hazards in Forested Areas,* R.C Sidle and M. Chigira, eds., Centre for Agriculture and Biosciences International, in review, 2001.